

## Evolution of Magnetic Field Twist and Tilt in Active Region NOAA 10930

B. Ravindra

*Indian Institute of Astrophysics,  
Koramangala, Bengaluru-560034  
E-mail: ravindra@iiap.res.in  
www.iiap.res.in*

P. Venkatakrishnan\* and Sanjiv Kumar Tiwari

*Udaipur Solar Observatory,  
Dewali, Badi Road, Udaipur-313001  
\*E-mail: pvk@prl.res.in*

Magnetic twist of the active region has been measured over a decade using photospheric vector field data, chromospheric  $H_{\alpha}$  data, and coronal loop data. The twist and tilt of the active regions have been measured at the photospheric level with the vector magnetic field measurements. The active region NOAA 10930 is a highly twisted emerging region. The same active region produced several flares and has been extensively observed by Hinode. In this paper, we will show the evolution of twist and tilt in this active region leading up to the two X-class flares. We find that the twist initially increases with time for a few days with a simultaneous decrease in the tilt until before the X3.4 class flare on December 13, 2006. The total twist acquired by the active region is larger than one complete winding before the X3.4 class flare and it decreases in later part of observations. The injected helicity into the corona is negative and it is in excess of  $10^{43}$   $Mx^2$  before the flares.

*Keywords:* Magnetic Helicity; Active Region; Sun

### 1. Introduction

It is generally believed that the magnetic fields on the sun is generated underneath the convection zone and they rise due buoyancy into the photosphere. Active region magnetic fields emerge as  $\Omega$  shaped fluxtubes at the photosphere. These emerged magnetic fields always exhibit some amount of twist. Twist is shearing of the field lines about its axis. Leka et al.<sup>1</sup> have found that the twisted emerging flux carries a current along with it. The

twist in the active region can originate due to several reasons. In the sub-photosphere, the field lines could twist due to the magnetic forces that are internal to fields. The generated magnetic fields can be twisted during the dynamo processes.<sup>2</sup> The generated field while rising through the convection zone is influenced by the convective buffeting that can introduce the twist in the field lines.<sup>3</sup> In the photosphere, the differential rotation of the sun can also introduce the twist, though in small amount.<sup>4</sup> The shearing motion of the magnetic footpoints can also twist the field lines at the photosphere after the emergence.

The parameter  $\alpha$  appear in the force-free field equation  $\nabla \times B = \alpha B$  is considered as a proxy for the twist.<sup>5</sup> Active region twist exhibits a hemispheric helicity rule, that is left/right handed twist in the northern and southern hemisphere.<sup>6,7</sup> However, many researchers now believe that the hemispheric helicity rule has to be re-investigated due to inconsistencies reported for different phases of solar cycles.<sup>8-10</sup>

Tilt is the angle made by the line joining the centroids of two opposite polarity with the solar equator. Many researchers considered the tilt as a proxy for the writhe of a fluxtube. The writhe is the spatial deformation of the flux tube around its axis. The tilt of the active region also follows the hemispheric rule that is positive in the northern and negative in the southern hemisphere, following the Hale-Nicholson law.<sup>11</sup> The tilt also depends on the latitude and is known as Joy's law.<sup>12</sup> The twist and writhe is interchangeable and their sum is a conserved quantity.<sup>13</sup>

The twist parameter is an interesting quantity in emerging active region.<sup>14</sup> Pevtsov et al.<sup>14</sup> have observed that the  $\alpha$  increases as the active region emerges and reaches a constant value after a day of the flux emergence. As the flux emerges into the photosphere, the coronal helicity increases. The accumulated helicity in the corona plays an important role in the energetic events such as flares and coronal mass ejections. Nandy et al.<sup>15,16</sup> have studied the relaxation of the twist towards constant  $\alpha$  force-free fields after flares. Nindos and Andrews<sup>17</sup> relate the coronal magnetic field line twist to eruptive and non-eruptive events.

The active region NOAA 10930 is well studied for twist,<sup>18</sup> flares<sup>19</sup> etc. In this paper, we would like to show how the twist and tilt of the active region varies over the time. Also, we would like to investigate, if there is any changes in the twist during the flare or CME. We used  $\alpha_{mean}$  as a parameter to study the twist in the active region. In the next section, we describe the vector magnetogram data utilized in this study and in Section 3, we present the results on how the twist and tilt evolves with time. In

Section 4, we present our conclusions.

## 2. Observational Data and Its Analysis

The spectro-polarimeter is one of the back-end instruments in solar optical telescope (SOT<sup>20–22</sup>) on board HINODE<sup>23</sup> satellite that makes spectropolarimetric measurements at a spatial sampling of  $0.3''$  in fast mapping mode and  $0.16''$  in normal mode. The Stokes I, Q, U and V spectra in Fe I 6301.5 Å and 6302.5 Å lines are obtained. It makes a map of the active region by spatial scanning of the slit positions. The spatial resolution along the slit direction is  $0.295''$  and in the scanning direction is  $0.317''/\text{pixel}$ . The obtained data set consists of total 36 vector magnetograms and is a mixer of both the modes. The obtained Stokes signals are calibrated using the standard solar software pipeline for the spectropolarimetry. The complete information on the vector magnetic fields is obtained by inverting the Stokes vector using the Milne Eddington inversion.<sup>24–26</sup> The ambiguity in the transverse field is resolved based on the minimum energy algorithm developed by Metcalf<sup>27</sup> and Leka.<sup>28</sup> The transformation of the magnetic field vectors to the heliographic coordinates has also been done.<sup>29</sup> The error in vertical ( $B_z$ ) and transverse field ( $B_t$ ) measurement is 8 G and 23 G, respectively.

Several methods have been developed to measure the twist in the active region magnetic fields. Almost all methods are based on the force-free parameter  $\alpha$ . The  $\alpha_{best}$  was introduced by Pevtsov.<sup>6</sup> This is the value of alpha for which the computed transverse field is best matched with the observed transverse field for whole active region and is called as  $\alpha_{best}$ . The other methods to measure the overall twist in the active region magnetic fields are (a) average value of  $\alpha$  computed for overall active region magnetic field,  $\alpha_{mean}$ <sup>30</sup> (b) global alpha,  $\alpha_g$  and (c) peak value of  $\alpha$  in the active region,  $\alpha_{peak}$ .<sup>31</sup> Apart from these, there is one more method that has been introduced in the literature known as signed shear angle (SSA).<sup>10</sup>

In this paper, we use the method of  $\alpha_{mean}$  to measure the twist in the active region NOAA 10930. We express the total twist in the emerging bipole region as a product of a magnetic coronal loop length ( $l$ ) and the winding rate ( $q$ ). If one takes the coronal loop as a semicircle of length ' $l$ ' then the circumference of the semicircle is  $\pi d/2$ . Where  $d$  is the distance between the flux weighted centroids of the two poles. The winding rate  $q$  is related to the twist parameter as  $\alpha_{mean}/2$ . Then the total twist is the

product of  $lq^{31,32}$  and is given by,

$$T = \frac{\pi d \alpha_{mean}}{2} \quad (1)$$

The tilt angle is computed by measuring the tilt of the line joining the flux weighted centroids of positive and negative poles in the counter-clockwise direction with respect to the equator. The east side of the line joining the equator is zero and the west side is  $180^\circ$  with values increasing in the counter-clockwise direction as a measure of tilt in the active region NOAA 10930. The pixels with vertical field strength values larger than 100 G is utilized in computing the centroid. This is to avoid the small scale features and noisy pixels.

The alpha maps have been obtained by first computing the vertical current density as

$$J_z(x, y) = \frac{1}{\mu} \left( \frac{dB_y}{dx} - \frac{dB_x}{dy} \right) \quad (2)$$

once the vertical current density is estimated then the vertical component of the twist parameter is computed through the relation between  $\alpha_z$ ,  $J_z$ , and  $B_z$  as,

$$\alpha_z(x, y) = \mu_0 \frac{J_z}{B_z} \quad (3)$$

where,  $B_z$  is the vertical component of the magnetic field in heliographic co-ordinate system and  $\mu_0$  is the permeability of free space and its value is  $4\pi \times 10^{-3} \text{ G mA}^{-1}$ . To avoid the pixels with zero  $B_z$ , that always occur near the neutral line, we have used a threshold of 100 G for  $B_z$ . The  $\alpha_z$  map is useful for finding the evolution of twist in space and time.

It is found that the measured twist ( $\alpha_z$ ) at the photosphere closely agrees with the coronal field line twist ( $\alpha_{corona}$ ).<sup>5</sup> In order to compute the coronal helicity we followed the results obtained by Berger<sup>33</sup> and implemented to the observed magnetograms as done by D emoulin et al.<sup>34,35</sup> The relative magnetic helicity, using a constant alpha force free method in the linearized form is given by,

$$H_r = \alpha \sum_{n_x=1}^{N_x} \sum_{n_y=1}^{N_y} \frac{|\tilde{B}_{n_x, n_y}^2|}{(k_x^2 + k_y^2)^{3/2}} \quad (4)$$

where,  $\tilde{B}_{n_x, n_y}$  is the Fourier amplitude of the longitudinal component of the magnetic field,  $k_x = 2\pi n_x/L$ ,  $k_y = 2\pi n_y/L$ , and L is the length of the computational window in the horizontal axis. The original form of the

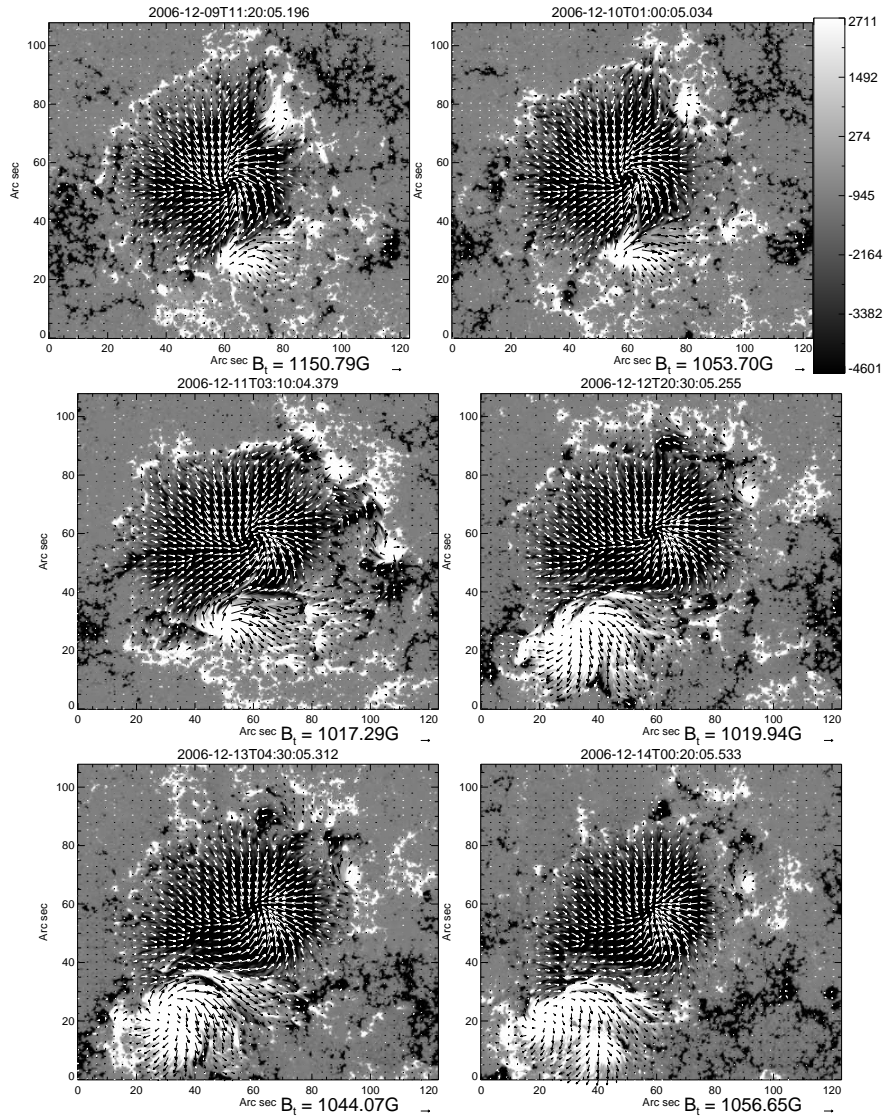


Fig. 1. The vector magnetograms are shown for each day. The background black (white) color represents the S (N) polarity regions of the vertical magnetic field strength ( $B_z$ ). The arrows represents the transverse field vectors overlaid upon  $B_z$ . The size of the arrow at the bottom of each figure indicates the magnitude of the transverse field and the vertical bar on the top right figure shows the magnitude of  $B_z$  expressed in G.

equation, its limitations and its simplification to the above form can be found in D emoulin et al.<sup>34</sup> In estimating the coronal helicity we used the  $\alpha_{mean}$  as the value for  $\alpha$  in the above equation.

### 3. Results

The active region NOAA 10930 appeared in the declining phase of the solar cycle 23<sup>rd</sup> in southern hemisphere at a latitude of 5°. The active region had two polarities when it appeared on the east limb on December 5, 2006 and they were almost aligned perpendicular to the East-West direction. It still survived when it crossed the west limb on December 17.

#### 3.1. Magnetic Flux

Figure 1 show the sample images of transverse field vectors overlaid upon  $B_z$  for each day of observations. In the vector field maps (as shown in Figure 1) it is clear that field lines are twisted. Both the polarities are located close to each other and boundary between the two is highly sheared. The N-polarity region was small on December 09, 2006 and it evolved over a period of 7 days.

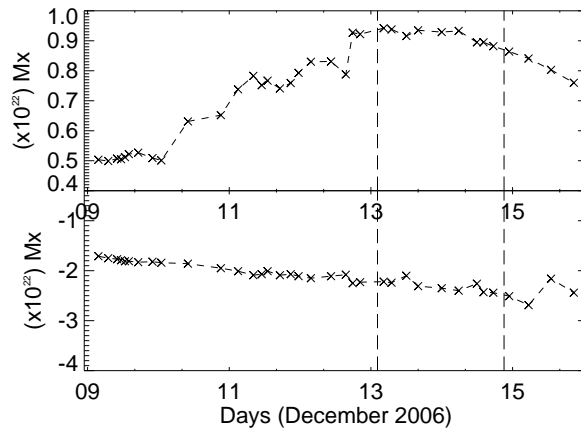


Fig. 2. The temporal evolution of magnetic flux is shown as a function of time. Top: N-polarity, Bottom: S-polarity.

Figure 2 shows the temporal evolution of flux over a period of 7 days. From the plot it is clear that there is a large imbalance in flux in the N and S-polarities. A vertical dashed lines in the plot represents the time of X3.4 and

X1.5 class flares that occurred on Dec 13, 2006 at 02:30 UT and Dec 14, 2006 at 21:07 UT respectively. The flux in the N-polarity region continuously increased until the X3.4 class flare occurred. It remained almost constant for sometimes and decreased subsequently.

### 3.2. *Twist in Active Region*

Twist is not distributed uniformly over the sunspot. In order to see where exactly the contribution to the overall twist is coming from, we have made the  $\alpha_z$  maps. In  $\alpha_z$  maps, it is easy to see that there is a mixed  $\alpha$  in the penumbra as seen by Su et al.<sup>10,18</sup> There is also salt-pepper like mixed alpha in the umbra. However, a dominant negative sign of  $\alpha$  is present in the emerging region, the N-polarity sunspot and also in a small portion of S-polarity sunspot. These dominant negative sign of  $\alpha$  in S and N-polarity region is shown by arrows in top-left of Figure 3. This dominant negative sign of twist can also be seen in all the subsequent maps made at different times in both the N and S-polarities. In the N-polarity region, the area of the dominant negative sign in  $\alpha$  increases with time till Dec 12 and later it decreases in size.

Figure 4(left) shows the plot of total twist ( $\star$ ) and tilt ( $\times$ ) expressed in terms of winding number. The total twist is estimated using the equation (1), and the number of windings is estimated as  $T/2\pi$ . From the plot it is clear that the total twist in the active region increases with time till the mid of Dec 12, 2006 and after that it starts to decrease with time. The active region has got more than one complete winding on Dec 11 which stays there till the mid of Dec 12, 2006. The dashed vertical lines in the plot indicate the time of X3.4 and X1.5 class flares. Before the X3.4 class flare the active region acquired about 0.8 turns and it reduced to 0.5 turns of the complete winding after the flare. Similarly, before the X1.5 class flare the active region has got close to one complete turn, and it decreased to 0.4 after the flare. We have estimated the error in measuring the total twist by varying the thresholds in  $B_z$  from 50 to 250 G in steps of 50 G. We estimated the mean value of total twist for those pixels whose value exceeds the thresholds in  $B_z$ . With this method we estimated the error in measuring the total twist and it is found to be less than 5%. This small variations in total alpha will not affect our results. Apart from these, we also examine the temporal variations in total twist using the another method called  $\alpha_g$  and found a similar variations in the total twist as a function of time.

The  $\times$  symbol in Figure 4(left) indicates the tilt of the active region with respect to the E-W direction. It started to decrease from the beginning

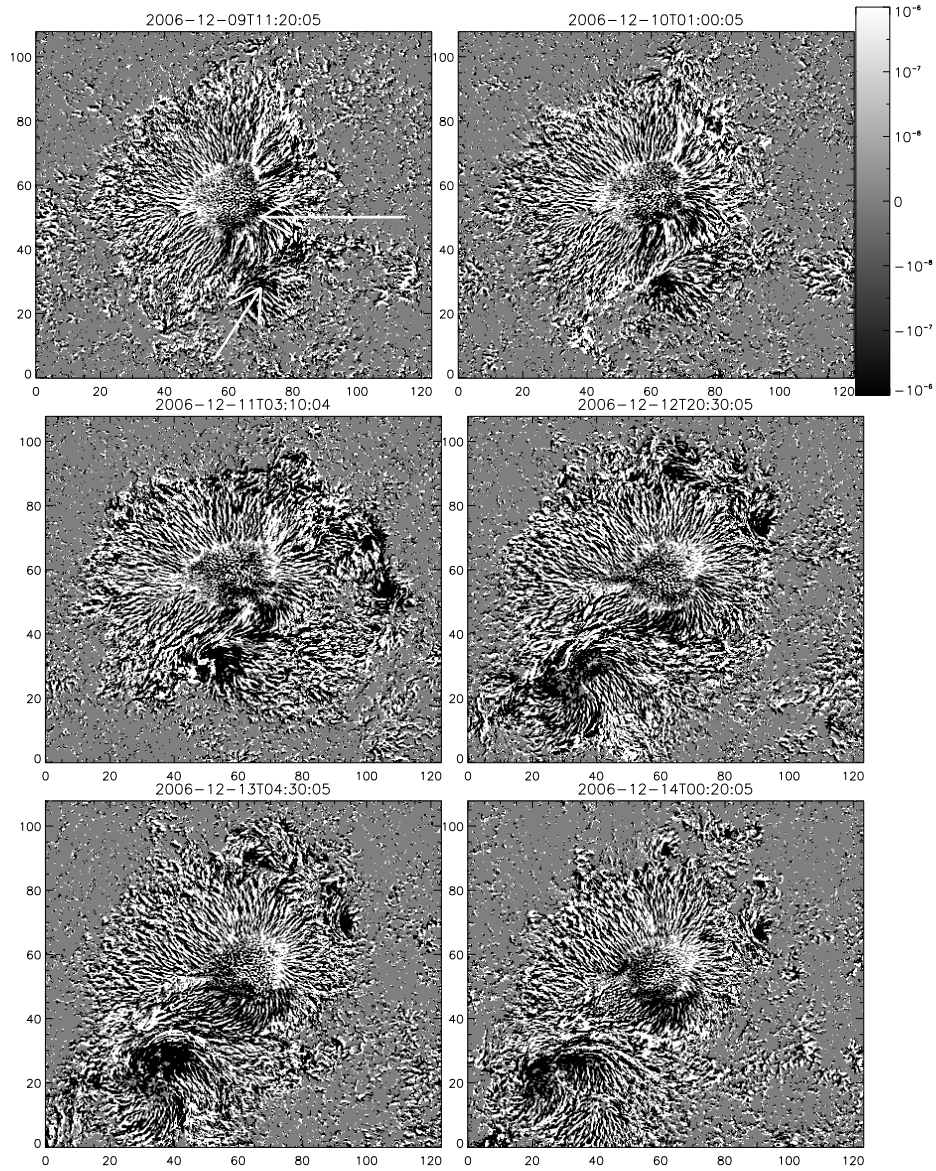


Fig. 3. The  $\alpha$  map is shown for each day of observations. The x-and y-axis are in arc sec units. The arrows in the top left image shows the dominant negative sign of alpha. The vertical bar on the top right figure shows the range of alpha in units of  $m^{-1}$ .



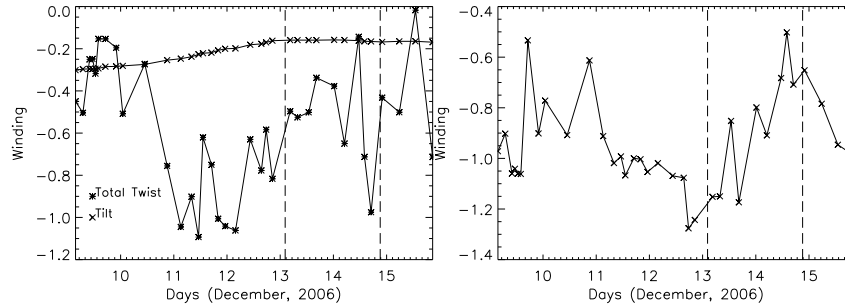


Fig. 4. The Total twist and tilt expressed in terms of winding number. Left: For the active region as a whole. Right: For the N-polarity region alone.

of the observation till the beginning of the X3.4 class flare. It attained almost constant value after the X3.4 class flare until the end of December 15, 2006. The tilt and twist behaved exactly opposite from December 9, 2006 till December 12, 2006. However, they differ in their magnitudes. This behavior is similar to the results obtained by Holder et al<sup>36</sup> and Nandy.<sup>37</sup> However, in the present case as the total twist increased with time, the tilt decreased.

It has been observed that the emerging N-polarity was rotating in the anti-clockwise direction.<sup>38</sup> The other S-polarity did not display any rotation. In order to see how much the twist appeared in the N-polarity we have independently estimated the twist for the N-region. Figure 4(right) shows a plot of total winding of N-polarity over a period of 7 days. Similar to the total twist of whole active region, the N-polarity also exhibited the increase in total twist starting from December 9, 2006 till mid day of December 12, 2006. It accumulated more than one complete winding just before the X3.4 class flare. The winding reduced after the X3.4 class flare, however it was still larger than one complete winding. Later, the total twist decreased and before the X1.5 class flare it was just 3/4th of one complete winding. Again, after X1.5 class flare there is small amount of decrease in total twist. It should be noted here that this is a mean value of the  $\alpha_z$  taken from distribution of  $\alpha_z$ . This means that there is a value of  $\alpha_z$  larger than the mean value and lower than the mean value. It also indicates that a significant number of pixels show their total twist larger than one complete winding.

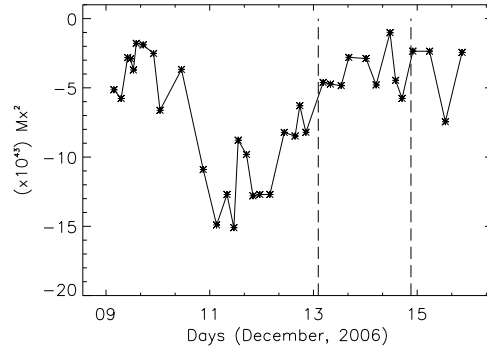


Fig. 5. A Plot of evolution of relative magnetic helicity as a function of time is shown here.

### 3.3. Relative magnetic helicity

Due to the emergence and rotation of sunspots, there is a large amount of helicity accumulated in the solar corona. There are several ways to estimate the relative magnetic helicity in the solar corona. Since the cadence of vector magnetic field data is small we cannot compute the velocity vectors required to estimate the relative helicity injection. Hence, we have used the eq (4) to estimate the coronal magnetic helicity. We have used the  $\alpha_{mean}$  as  $\alpha$  in the eq(4). Figure 5 shows a relative magnetic helicity plotted over a period of 7 days. The magnetic helicity curve follows the total twist curve. The injected helicity is very large. Before the X3.4 class flare it was  $7 \times 10^{43}$  Mx<sup>2</sup> which decreased to  $4 \times 10^{43}$  Mx<sup>2</sup> after the X3.4 class flare.

## 4. Conclusions

An increase in the flux and the total twist of the active region during first half of the observation suggests that a new flux region is emerging. This confirms that the emerging region carries current and twist generated below the photosphere along with it as observed by Leka et al.<sup>39</sup> The twist increased in the active region until the on-set of X3.4 class flare and showed a decreasing trend thereafter. A similar trend of increase and decrease in twist was noticed before and after the X1.5 class flare too. This suggests that the twist in the active region slowly relaxing towards the lower value.<sup>15</sup>

Leamon et al.<sup>32</sup> suggest that the coronal loops become unstable and erupt only when their total twist exceeds the critical twist,  $2\pi$ . However, in their study they do not find any active region exceeding this critical twist. Many active regions exhibit their total twist of about  $2\pi/3$  and some

of them even did not exceed  $2\pi/6$  value of one complete winding. In our observations, we find that the total twist exceeded one complete winding on December 11 and 12, 2006. However, it decreased just before the X3.4 class flare reaching 0.8 times one complete winding and before the X1.3 class flare it is close to one complete winding. This result was obtained when we take the active region as a whole. On the other hand, when we computed the total twist in the N-polarity region alone, it exhibited larger than one complete winding and it was about 1.3 times the 1-complete winding before the X3.4 class flare. It decreased to 1.1 turn after the X3.4 flare. However, before the X1.3 class flare the total twist was less than  $3\pi/4$  of 1-complete turn. This is only for the mean value of the total twist in the active region. However, the active region has a distribution of local twist ( $\alpha$ ) and many regions show larger twist than the mean of this distribution. This means that this active region shows more than one complete winding in many locations of the sunspots, exceeding the critical limit of  $2\pi$ . We do not know at this stage whether this active region erupted due to kink instability or due to some other reason. We need a coronal observations to find such kink instability. At present, from this study it appears that there is a decrease in the total twist after the flare. In order to firmly establish the role of critical twist in the eruptive X and M class flares, we need to observe many such events.

## 5. Acknowledgments

We thank the two unknown referees for their useful comments which improved the presentation in the manuscript. Hinode is a Japanese mission developed and launched by ISAS/JAXA, with NAOJ as domestic partner and NASA and STFC (UK) as international partners. It is operated by these agencies in co-operation with ESA and the NSC (Norway).

## References

1. K. D. Leka, Y. Fan and G. Barnes, *ApJ*, **626**, 1091, 2005.
2. P. A. Gilman and P. Charbonneau, in *Magnetic Helicity in space and Plasmas*, ed. M. R. BBrown, R. C. canfield and A. A. Pevtsov, *Geophys. Monograph.*, **111**, Washington DC: AGU, 75.
3. D. W. Longcope, G. H. Fisher and A. A. Pevtsov, *ApJ*, **507**, 417, 1998.
4. C. R. DeVore, *ApJ*, 539, 944, 2000.
5. A. B. Burnette, R. C. Canfield and A. A. Pevtsov, *ApJ*, **606**, 565, 2004.
6. A. A. Pevtsov, R. C. Canfield and T. R. Metcalf, *ApJ*, **440**, 109, 1995.
7. D. M. Rust and A. Kumar, *ApJ*, **464**, 199, 1996.
8. M. Hagino and T. Sakuri, *PASJ*, **57**, 481, 2005.

9. A. A. Pevtsov, R. C. Canfield., T. Sakurai, and M. Hagino, *ApJ*, **677**, 719, 2008.
10. S. K. Tiwari, P. Venkatakrishnan, and K. Sankarasubramanian, *ApJ*, **702**, 133, 2009.
11. G. E. Hale, F. Ellerman, S. B. Nicholson and A. H. Joy, *ApJ*, **49**, 153, 1919.
12. H. Zirin, *The Solar Atmosphere* (Cambridge University Press. Cambridge).
13. G. Călugăreanu, 1959, *Rev. Math. Pures Appl.*, **4**, 5, 1959.
14. A. A. Pevtsov, V. M. Maleev and D. W. Longcope, *ApJ*, **593**, 1217, 2003.
15. D. Nandy, M. Hahn, R. C. canfield, and D. W. Longcope, *ApJ*, **597**, 73, 2003.
16. M. Hahn, S. Gaard, J. Patricia, R. C. Canfield, D. Nandy, *ApJ*, 629.1135, 2005.
17. A. Nindos and M. D. Andrews, *ApJ*, **616**, 175, 2004.
18. J. T. Su, T. sakurai, Y. Suematsu, M. Hagino, Y. Liu, *ApJ*, **697**, 103, 2009.
19. H. Isobe, et al. *PASJ*, **59**, 807, 2007.
20. S. Tsuneta et al. 2008, *Solar Phys.*, **249**, 167, 2008.
21. Y. Suematsu et al. 2008, *Solar Phys.*, **249**, 197, 2008.
22. K. Ichimoto et al. 2008, *Solar Phys.*, **249**, 233, 2008.
23. T. Kosugi et al. *Solar Phys.*, **243**, 3, 2007.
24. A. Skumanich and B. W. Lites, *ApJ*, **322**, 473, 1987.
25. B. W. Lites and A. Skumanich, *ApJ*, **348**, 747, 1990.
26. B. W. Lites, D. F. Elmore, P. Deagraves and A. P. Skumanich, *ApJ*, **418**, 928, 1993.
27. T. R. Metcalf, *Solar Phys.*, **155**, 235, 1994.
28. K. D. Leka, *ASPC*, **415**, 365, 2009.
29. P. Venkatakrishnan, M. J. Hagyard, and D. H. Hathaway, *Solar Phys.*, **115**, 125, 1988.
30. M. Hagino and T. Sakurai, *PASJ*, **56**, 831, 2004.
31. K. D. Leka, Y. Fan and G. Barnes *ApJ*, **626**, 1091, 2005.
32. R. J. Leamon, R. C. Canfield, Z. Blehm and A. A. Pevtsov, *ApJ*, **596**, 255, 2003.
33. M. A. Berger, *ApJS*, **59**, 433, 1985.
34. P. Démoulin, C. H. Mandrini, van Driel-Gesztelyi, B.J. Thompson, S. Plunckett, Z. Kovári, G. Aulanier and A. Young, *A&A*, **382**, 650, 2002.
35. P. Démoulin, *Adv. Spa.Res.*, **39**, 1674, 2007.
36. Z. A. Holder, R. C. Canfield, R. A. McMullen, D. Nandy, R. F. Howard, and A. A. Pevtsov, *ApJ*, **611**, 1149, 2004.
37. D. Nandy, *JGR*, bf 111, A12S01, 2006.
38. S. Min and J. Chae, *Solar Phys.*, **258**, 203, 2009.
39. K. D. Leka, R. C. Canfield, A. N. McClymont and L. van Driel-Gesztelyi, *ApJ*, **462**, 547, 1996.